Available online at www.sciencedirect.com
SCIENCE DIRECT®
International Journal of Heat and Fluid Flow 24 (2003) 785–794
International Journal of HEAT AND FLUID FLOW
www.elsevier.com/locate/ijhff

Investigation of the influence of the Reynolds number on a plane jet using direct numerical simulation

M. Klein *, A. Sadiki, J. Janicka

Technische Universität Darmstadt, FG Energie- und Kraftwerkstechnik, Petersenstraße 30, 64287 Darmstadt, Germany

Received 8 July 2002; accepted 2 April 2003

Abstract

Free jets represent a benchmark for research into the physics of turbulent fluid flow and are furthermore of great interest for many engineering applications. In the present work we investigate the influence of the Reynolds number on the evolution of a plane jet. The effect on the global jet characteristics, as well as on some spectral properties, is particularly addressed. A strong influence on the jet evolution is found for $Re \leqslant 6000$, but also that the jet is close to a converged state for higher Reynolds numbers. Although it is believed that the jet reaches a universal self-similar state, there was early evidence that the inflow conditions can have a downstream effect on the development of the turbulent flow field. Therefore some results, concerning the influence of inflow boundary conditions on the simulations, are also reported.

Keywords: Plane jet; DNS; Reynolds number dependence; Inflow conditions

1. Introduction

Free jets represent a benchmark for research into the physics of turbulent fluid flow, because they are used for the evaluation of physical models. Furthermore they are of great interest for many engineering applications (jet propulsion, combustion chambers, etc.). Therefore turbulent jets have been the subject of many experimental and numerical works for over 40 years. For the axisymmetric jet the very extensive measurements of Wygnanski and Fiedler (1975) have been the standard round jet data for a long time. Later it was discovered by using numerical methods that the far field data of Wygnanski and Fiedler have not satisfied the constraint of the integrated axial momentum equation and that this discrepancy has been due to the semi-confined enclosure (Hussein et al., 1994). Nearly two decades later detailed measurements with more suitable measurement techniques have been carried out (Panchapakesan and Lumley, 1993; Hussein et al., 1994). In contrast to the round jet, according to Bonnet et al. (1998), detailed results newer than those from Gutmark and Wygnanski (1976) (denoted GW in the following) are not available for the plane jet, but in view of the above mentioned findings for the axisymmetric jet, the data of GW must be also cast in doubt.

There is little work about free jets at moderate Reynolds numbers, although it is for several reasons interesting to study the influence of the Reynolds number on the evolution of a plane jet. First the Reynolds number dependence might be a possible explanation for the large scatter in the experimental data. Secondly, experimental data or DNS data is frequently used for calibration, development and examination of turbulence closures models, which contain often no *Re*-dependence. Therefore Reynolds-dependant data could be useful (1) for determining the range where these models can be valid or (2) alternatively provide necessary information for a model refinement. From this point of view it is of great importance to be able to predict very well the flow field evolution and the distribution of the mixing field in such a configuration.

An overview of the computational studies concerning this flow can be found in the work of Stanley et al.

* Corresponding author. Tel.: +49-6151-162457; fax: +49-6151-166555.
E-mail addresses: kleinm@hrzpub.tu-darmstadt.de (M. Klein), sadiki@ekt.tu-darmstadt.de (A. Sadiki), janicka@ekt.tu-darmstadt.de (J. Janicka).

0142-727X/$ - see front matter © 2003 Elsevier Inc. All rights reserved.
doi:10.1016/S0142-727X(03)00089-4

(2002), who published a study of the flow field evolution and mixing in a planar turbulent jet at $Re = 3000$, using DNS. The inflow conditions were generated by a procedure based on inverse Fourier transform.

Based on a newer method of generating realistic inflow conditions presented in Klein et al. (2003), the present work extends previous simulations by varying the Reynolds number.

In the following section we recall the governing equations and the numerical technique needed for the simulations. After that the new method of generation of artificial inflow data is summarized in Section 3. In the main part of the paper (Section 4) we then discuss computational and physical aspects of the plane jet. Starting with the influence of the inflow conditions, we proceed with the far field results of the jet and present at the end of the section some results reflecting the effects of Reynolds number variations. Finally some conclusions will close the paper.

2. Governing equations and numerical technique

The governing equations for the problem to be investigated here, are the conservation equations of mass and momentum in their instantaneous, local form:

$$\frac{\partial u_i}{\partial x_i} = 0 \tag{1}$$

$$\frac{\partial}{\partial t}(\rho u_i) = -\frac{\partial}{\partial x_j}(\rho u_i u_j) + \frac{\partial}{\partial x_j}\mu\left(\frac{\partial u_i}{\partial x_j} + \frac{\partial u_j}{\partial x_i}\right) - \frac{\partial p}{\partial x_i} \tag{2}$$

The incompressible Navier–Stokes-equations are solved by using a finite volume technique on a cartesian mesh. The variables are located on a staggered grid. For spatial discretization central differences are used. Temporal discretization is an explicit third order Runge–Kutta-method. The Poisson equation is inverted by using a direct fast elliptic solver.

The turbulent plane jet is simulated with a Reynolds number $Re = U_0 D/v$ in the range from 1000 to 6000, where U_0 denotes the bulk velocity at the inlet, D the nozzle width and v the kinematic viscosity. A sketch of the flow can be seen in Fig. 1 together with the definition of the jet half-width $z_{1/2}$ and the centerline velocity U_{cl}. The extension of the computational domain in axial (x), homogenous (y) and vertical (z) direction is $20D \times 8D \times 20D$. The spanwise box size was estimated a priori using the experimental data of GW

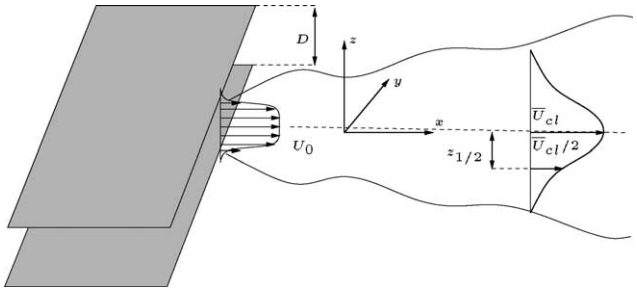

Fig. 1. Sketch of the flow.

$$z_{1/2} \approx 0.1D, \quad L_x/z_{1/2} = 0.47 \tag{3}$$

yielding an integral length scale at the outflow plane of approximately $1D$. Therefore the spanwise box size should be large enough to capture even the largest scales. This is confirmed a posteriori in Fig. 2(left). Compared with the computational box of Stanley et al. (2002) we added some safety overhead.

The computational domain is resolved with $360 \times 128 \times 512 \approx 23.4 \times 10^6$ grid points. In vertical direction the region $-4.5 \leqslant z/D \leqslant 4.5$ is resolved with 50 cells per diameter and the grid is stretched at the lateral boundaries. In x and y direction the grid is equidistant. This yields in the "core" region a resolution of $\Delta x/D = 1/18$, $\Delta y/D = 1/16$ and $\Delta z/D = 1/50$. The finer grid spacing in z direction is required to resolve well the shear layer, especially in the near nozzle region. The same grid is used for all simulations in order to be able to use exactly the same inflow data. Because we performed not only one DNS but several parameter variations, we had to reduce the amount of stored data (the complete velocity and pressure field for one time step takes in single precision 378 MB of memory). Therefore we are not able to

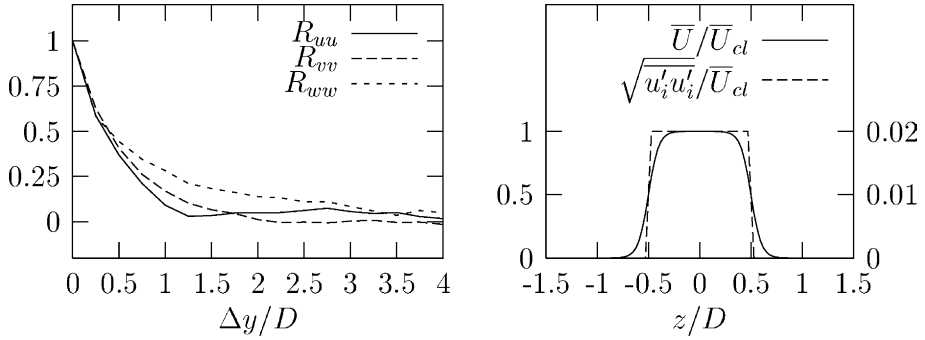

Fig. 2. Autocorrelation functions in homogenous direction at the last axial position ($x/D = 15$) which is used for evaluation (left). Inflow profiles for mean velocity and mean velocity fluctuations (right).

estimate the complete dissipation tensor. Using the isotropic assumption $\varepsilon = 15\nu(\partial u'/\partial x)^2$ we obtained for $Re = 4000$ the estimate $\eta_{\min}/D = 0.008$ at $x/D \approx 7$. The values for all other cases can be found using the proper Reynolds number scaling law, where it has to be mentioned that the maximum dissipation occurs closer to the nozzle, the higher the Reynolds number. Our findings agree astonishingly good with the results of Stanley et al. (2002), where the full dissipation tensor is evaluated.

The simulations are performed for 13 flow through times based on an averaged axial centerline velocity. All statistics are taken over 10 flow time units. The CPU time for one simulation is approximately 800 h on an Intel P4.

At the outflow, Neumann boundary conditions for the velocity and the pressure are prescribed, negative velocities are clipped. According to our experience, no notable difference can (in this case) be seen between the results obtained with Neumann boundary conditions and the results obtained with a convective outflow condition. Because the convective outflow condition yielded furthermore stability problems for the first time steps, where the flow had not reached a statistically stable state, we used simply Neumann boundary conditions. Setting the pressure to zero at the top and the bottom boundaries and interpolating the tangential velocities constantly allows for mass entrainment. Periodic boundary conditions are applied in the homogenous direction. At the inflow boundary the velocity is set to zero outside the nozzle. Thomas and Goldschmidt (1986) report that the velocity profile in the near nozzle region is closely approximated by a hyperbolic-tangent profile. For this reason inside the nozzle the mean velocity profile has been chosen according to

$$\overline{U} = \frac{U_0}{2} + \frac{U_0}{2}\tanh\left(\frac{-|z| + 0.5D}{2\theta}\right), \quad \overline{V} = \overline{W} = 0, \qquad (4)$$

where θ is the momentum thickness and has been set to $D/20$ as in Ribault et al. (1999). Because no reliable information about the profile of the velocity fluctuations close to the nozzle was available we used simply a top-hat profile with

$$\sqrt{\overline{u'u'}}/U_{\mathrm{cl}} = \sqrt{\overline{v'v'}}/U_{\mathrm{cl}} = \sqrt{\overline{w'w'}}/U_{\mathrm{cl}} = 0.02. \qquad (5)$$

The inflow profiles are also plotted in Fig. 2(right). In contrast to Stanley et al. (2002) the fluctuations have been generated by a new procedure presented in Klein et al. (2003). For the self-consistency of this paper, we summarize the method in the next section.

3. Generation of artificial inflow data

In the following we provide only a short introduction to the generation of inlet data for spatially developing simulations. For more details see e.g. Lund et al. (1998), Stanley and Sarkar (2000), Klein et al. (2003) and Glaze and Frankel (in press).

The conventional way to generate turbulent inflow data is to take a mean velocity profile with superimposed fluctuations. Using the numerical technique described in Section 2, a simulation of a plane jet at Reynolds numbers varying in the range from 1000 to 6000 has been performed in Klein et al. (2000). Although the results compared well with experimental data for self-similarity profiles, the jet spreading rate was under-predicted by approximately 20%. The most probable reason for this discrepancy seemed to be the influence of non-realistic inflow conditions.

In Fig. 3 we compare the axial evolution of the longitudinal velocity fluctuations from three simulations, which differ only in the inflow boundary conditions. A mean velocity profile from a channel flow simulations has been used with superimposed (1) zero fluctuations, (2) random fluctuations and (3) fluctuations from an external channel flow DNS.

It can be observed that due to a lack of energy in the low wave number range, the pseudo turbulence is immediately damped to zero, and the result is identical with a laminar inflow. Therefore this procedure is completely wrong. This explains a certain independence of the fluctuation level on the simulation results, when using 'white noise' fluctuations. In consideration of this fact the choice of laminar inflow conditions seems to be superior to the random fluctuation approach. Additionally if an iterative solver is used, the number of iterations can be reduced dramatically (see for example Mengler et al., 2001). The use of real turbulence, e.g. from an auxiliary simulation, at the inflow shows a complete different behavior. In this case the fluctuation level is maintained and increases up to the end of the potential core where the shear layer has penetrated into the jet up to the centerline. Unfortunately the spreading rate remains still considerably under-predicted.

As we have seen the direct numerical simulation of a plane jet requires an elaborated method for producing

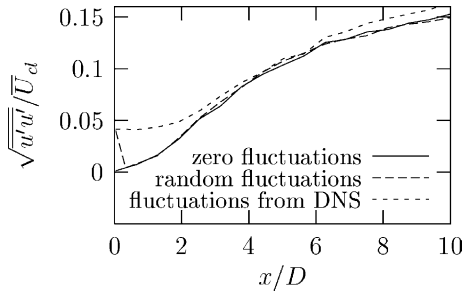

Fig. 3. Influence of conventional inflow boundary conditions on the simulation of a plane jet. Comparison between inflow with zero fluctuations, random fluctuations and fluctuations from an external channel flow DNS.

realistic inflow data. It is very difficult to specify the meaning of good inflow data, but a simple approach is to produce a velocity signal which has certain statistical properties, which may for example be known from experimental data. Such quantities could be: mean values, fluctuations and cross correlations, higher order moments, length and time scales, energy spectra, etc. Klein et al. (2003) developed a method which can be splitted in two parts.

1. First a provisional three-dimensional signal $\mathscr{U}_i$ is generated for each velocity component which possesses a prescribed two-point statistic (length scale, energy spectra). If there would only be the need to obtain homogenous turbulence the procedure could stop here.
2. If cross correlations between the different velocity components have to be taken into account a method proposed by Lund et al. (1998) can be used. First define $\mathscr{U}_i$ so that $\overline{\mathscr{U}_i} = 0$, $\overline{\mathscr{U}_i \mathscr{U}_j} = \delta_{ij}$ and then perform the following transformation: $u_i = \bar{u}_i + a_{ij}\mathscr{U}_j$, where

$$(a_{ij}) = \begin{pmatrix} (R_{11})^{1/2} & 0 & 0 \\ \dfrac{R_{21}}{a_{11}} & (R_{22} - a_{21}^2)^{1/2} & 0 \\ \dfrac{R_{31}}{a_{11}} & \dfrac{(R_{32} - a_{21}a_{31})}{a_{22}} & (R_{33} - a_{31}^2 - a_{32}^2)^{1/2} \end{pmatrix}.$$

Here $\overline{(\cdot)}$ denotes an appropriate averaging procedure, R_{ij} the correlation tensor which may be known from experimental data and u_i the finally needed velocity signal.

A method for the solution of part 1 has first been proposed by Lee et al. (1992). The idea is based on an inverse Fourier transform but has, according to our opinion some disadvantages which will be overcome by the new method based on digital filtering of random data, following the work of Nobach (1997).

Guideline for the development was the practicability, which means that only statistical quantities should be used which can be obtained with reasonable experimental expense, or alternatively from heuristical estimates. Therefore correlation functions respectively length scales seem to be an adequate alternative to a three-dimensional energy spectrum.

In order to create two-point correlations, let r_m be a series of random data with $\overline{r_m} = 0$, $\overline{r_m r_m} = 1$, then

$$u_m = \sum_{n=-N}^{N} b_n r_{m+n} \tag{6}$$

defines a convolution or a digital linear non-recursive filter. The b_n are the filter coefficients and N is connected to the support of the filter. Because $\overline{r_m r_n} = 0$ for $m \neq n$ it follows easily

$$\frac{\overline{u_m u_{m+k}}}{\overline{u_m u_m}} = \sum_{j=-N+k}^{N} b_j b_{j-k} \Bigg/ \sum_{j=-N}^{N} b_j^2, \tag{7}$$

that means a relation between the filter coefficients and the autocorrelation function of the u_m. Two questions have to be answered: How can this procedure be extended to three dimensions and how is it possible to invert formula (7). By the convolution of three one-dimensional filters one obtains a three-dimensional filter that answers the first question:

$$b_{ijk} = b_i \cdot b_j \cdot b_k \tag{8}$$

To find an answer to the second problem, lets suppose an autocorrelation function is given, i.e. $\overline{u_m u_{m+k}}/\overline{u_m u_m}$. Then it is possible to obtain the coefficients b_n by a multidimensional Newton method. The procedure can be taken from a standard textbook and needs no further comment.

In contrast to the knowledge of the full autocorrelation function one has often an intuitive feeling for the length scale of a flow. Therefore we propose a further simplification, which is especially preferable from an engineering point of view: instead of $R_{uu}(\boldsymbol{x}, \boldsymbol{r})$, where $\boldsymbol{r}$ denotes a distance vector and $r = |\boldsymbol{r}|$, only an integral value, the length scale, should be prescribed. This implies the assumption of a special shape of R_{uu}. For the case of homogeneous turbulence in a late stage, it can be shown (Batchelor, 1953) that the autocorrelation function takes the form

$$R_{uu}(r,0,0) = \exp\left(-\frac{\pi}{4}\frac{r^2}{L^2}\right) \quad (\text{with } L = L(t) = \sqrt{2\pi\nu(t-t_0)}) \tag{9}$$

This choice fulfills some basic properties like $R_{uu}(0) = 1$, $\lim_{r\to\infty} R_{uu}(r) = 0$, and allows an easy calculation of the length scale. In particular an explicit representation of the filter coefficients has been found. Suppose Δx is the grid spacing and $L = n\Delta x$ the desired length scale, then we can set

$$\frac{\overline{u_m u_{m+k}}}{\overline{u_m u_m}} = R_{uu}(k\Delta x) = \exp\left(-\frac{\pi}{4}\frac{(k\Delta x)^2}{(n\Delta x)^2}\right) = \exp\left(-\frac{\pi}{4}\frac{k^2}{n^2}\right) \tag{10}$$

with the filter coefficients

$$b_k \approx \tilde{b}_k \Bigg/ \left(\sum_{j=-N}^{N} \tilde{b}_j^2\right)^{1/2} \quad \text{and}$$

$$\tilde{b}_k := \exp\left(-\frac{\pi}{2}\frac{k^2}{n^2}\right) \tag{11}$$

Formula (11) is only approximatively valid, but numerically the following error estimate can be given:

$$\max_k \left| \exp\left(-\frac{\pi}{4}\frac{k^2}{n^2}\right) - \sum_{j=-N+k}^{N} b_j b_{j-k} \Big/ \sum_{j=-N}^{N} b_j^2 \right| \leqslant 0.001$$
$$\text{for } N \geqslant 2n \text{ and } n = 2, \ldots, 100 \qquad (12)$$

That means the support N should be large enough to capture twice the length scale which anyway makes sense because otherwise the correlation is truncated to zero before approaching the x-axis. If a spatial dependence of the b_k is allowed it is even possible to vary the length scale spatially, for example in a wall bounded flow. Normally we generated the inflow data on the fly, but alternatively it would be also possible to store a large volume of data and to convect it through the inflow plane by applying Taylors hypothesis. More details as well as some validation results of the procedure can be found in Klein et al. (2003).

4. Results and discussion

In this section we discuss some computational and physical aspects of the plane jet. Starting with the influence of the inflow length scale, we proceed with the far field results of the jet. At the end of the section we study in detail the effects of the variation of the Reynolds number on the jet evolution.

4.1. Influence of the inflow length scale

Many experimental studies use a contraction nozzle and therefore report a top-hat profile for the mean velocity. In combination with the inflow generator this yields a realistic inflow boundary condition, as we will see below. For the simulations carried out here, velocity profiles with a fluctuation level of 2% have been generated by the procedure presented above. These fluctuations were superimposed to the smoothed top-hat profile (4).

Due to the observation (see Klein et al., 2001) that the distribution of the kinetic energy from the inflow data onto different length scales has an important impact on the evolution of the jet at least in the near field, we studied this influence systematically. Under the assumption that the autocorrelation function has a Gaussian shape, it is now very simple to produce inflow data with different length scales. In Fig. 4 the length scale has been varied in the range from $1/6D$, $2/6D$, $4/6D$. As expected the jet spreading rate increases, the more kinetic energy is put into the large scales.

Comparing the axial evolution of the longitudinal fluctuations in Fig. 4 with the random fluctuations in Fig. 3 it is obvious that the data from the inflow generator is much closer to real turbulence.

4.2. Far field results

It is often assumed that the jet reaches downstream a universal self-similar state. Therefore the lateral profiles in this section are as usual normalized with the local centerline velocity U_{cl} and the jet half-width $z_{1/2}$. We summarize in the following the far field results for the turbulent jet with $Re = 4000$. The length scales at the inflow have been set to $0.4D$, $0.125D$, $0.125D$ in x, y, z direction according to the channel flow measurements reported in Hinze (1959). Fig. 5 shows the broadband inflow forcing at $x/D = 0$ together with temporal energy spectra for $Re = 4000$ at two further characteristic axial positions: The coherent structures in the near field at $x/D = 2.5$ (see also Fig. 10) and a spectrum in the self-similar region of the jet at $x/D = 12.5$.

All data has been averaged over approximately 10 flow through times based on a mean axial velocity. Because the outflow boundary conditions have an upstream influence on the jet, all quantities are evaluated only for $x/D \leqslant 15$.

We compare our results with the DNS data of Stanley et al. (2002) and the experimental data of Gutmark and Wygnanski (1976) and Namer and Ötügen (1988), denoted in the following SSM, NÖ and GW. As already pointed out in Bonnet et al. (1998), the results of GW for the plane jet, must be cast in doubt at least for the longitudinal fluctuations (compare also Fig. 7(left)). Unfortunately in the newer data set of NÖ performed for $Re = 1000$–7000 compared to $Re = 30000$ in GW,

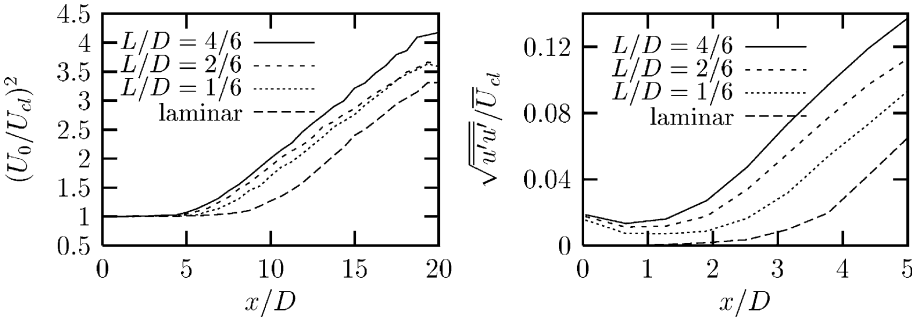

Fig. 4. Influence of different length scales (imposed at the inflow) on the development of a plane jet: velocity decay (left), velocity fluctuations (right).

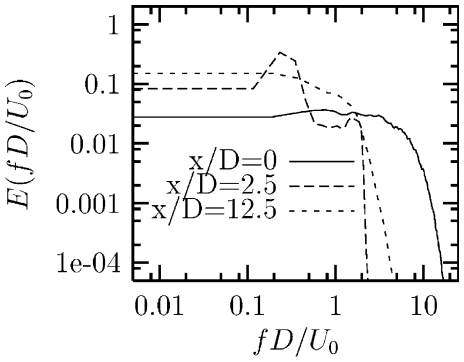

Fig. 5. Temporal energy spectrum for $Re = 4000$ at characteristic axial positions.

the fluctuations v_{rms}, w_{rms} as well as the shear stress are not included. Although our numerical findings lie very well in the range of the experimental data, it must be mentioned and has to be kept in mind, that the experimental scatter is very large (see Table 1). For example the values for the velocity decay constant C_u reach from 0.093 to 0.22.

Fig. 6 shows the axial mean velocity. It is very well represented by a Gaussian profile

$$\frac{U(z)}{U_{\mathrm{cl}}} = \exp\left[-C\left(\frac{z}{z_{1/2}}\right)^2\right] \tag{13}$$

with $C \approx 0.683$ and agrees well with the data of NÖ. Compared to GW a notable discrepancy is found for $z/z_{1/2} \geqslant 1.5$. Also the lateral mean velocity is reasonably represented by the experimental data of GW, although the profiles do not yet collapse to a single curve. For the longitudinal velocity fluctuations shown in Fig. 7(left), the situation is different. The DNS supports the observation mentioned in Bonnet et al. (1998) that the results from GW were considerably overestimated, especially in the shear layer. A good agreement with NÖ is found. Whereas the centerline value of the spanwise fluctuations is quite well predicted, an overshoot of $\overline{v'v'}$ in the shear layer can be seen, which is also apparent in the data of Stanley et al. (2002).

Fig. 8(left) shows the lateral velocity fluctuation as well as the shear stress (right). They agree reasonably well with the experimental findings of GW. Comparing the first mentioned quantity to GW, it can be seen that $\overline{w'w'}$ decreases slower with increasing $z/z_{1/2}$. This is also observed in the data of Stanley et al. (2002), but it has to be mentioned that their centerline value is approximately 30% higher. The deviation between both DNS data sets is perhaps due to different inflow conditions or due to the fact that Stanley et al. (2002) consider a plane jet with a weak coflow.

4.3. Variation of the Reynolds number

It is for several reasons interesting to study the influence of the Reynolds number on the evolution of a plane jet. First the Reynolds number dependence might be a possible explanation for the large scatter in the

Table 1
Axial and lateral centerline fluctuation level u_{rms}, w_{rms}, velocity decay C_u, spreading rate C_z

Author	u_{rms}/U_0	w_{rms}/U_0	C_u	C_z
Gutmark and Wygnanski (1976)	0.27	0.206	0.188	0.1
Thomas and Goldschmidt (1986)	0.27	–	0.22	0.1
Hussain and Clark (1977)	0.19	–	0.123	0.118
Namer and Ötügen (1988)	0.22	–	0.175	0.098
Ramaprian and Chandrasekhara (1985)	0.2	0.17	0.093	0.112
Thomas and Prakash (1991)	0.245	0.22	0.22	0.11
DNS Stanley et al. (2002)	0.255	0.264	0.201	0.092
Present DNS results ($Re = 6000$)	0.23	0.20	0.178	0.106

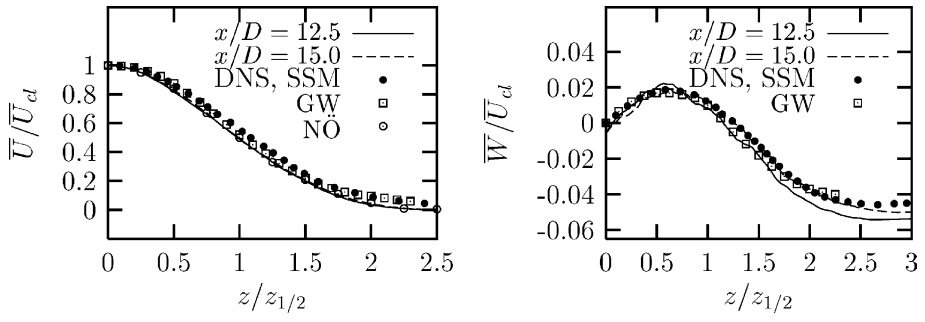

Fig. 6. Mean velocity in axial and lateral direction.

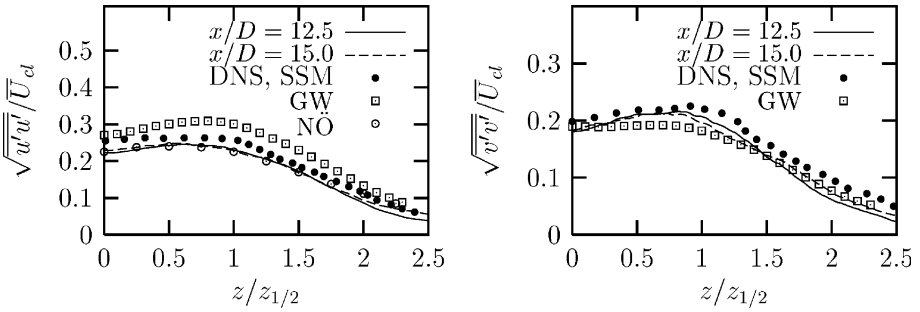

Fig. 7. Fluctuations in axial and homogeneous direction.

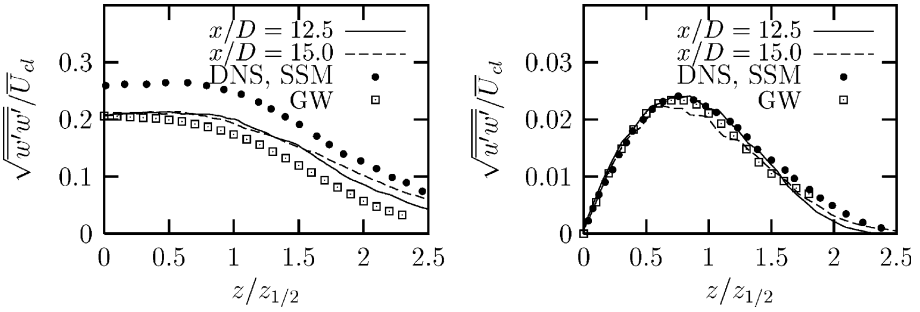

Fig. 8. Fluctuations in lateral direction and shear stress.

experimental data. Secondly, experimental data or DNS data is frequently used for calibration, development and examination of turbulence closures models, which often contain no *Re*-dependence. Therefore such data could be useful for determining the range where these models can be valid or alternatively could provide necessary information for a model refinement. We examine first the variation of the global jet characteristics and then consider some spectral properties of the flow for different Reynolds numbers.

First we fitted the parameter C in (13) to our computed mean longitudinal velocity profiles. Table 2 shows that independent of the Reynolds number u/U_{cl} is closely approximated by formula (13) with $C \approx \ln 2$. This is the same finding as reported in NÖ.

The profiles presented in the last section are as usual normalized with U_{cl} and $z_{1/2}$, due to the assumption that the jet reaches a self-similar state. Furthermore it is believed that the centerline velocity decays like

$$\left(\frac{U_0}{U_{cl}}\right)^2 = C_u\left(\frac{x}{D} - C_{u,0}\right) \tag{14}$$

Table 2
Fitted coefficient C, see formula (13)

Re	1000	2000	4000	6000
C	0.695	0.677	0.692	0.668

and the jet spreads linearly with x, i.e.

$$\frac{z_{1/2}}{D} = C_z\left(\frac{x}{D} - C_{z,0}\right). \tag{15}$$

To assess the absolute error it is therefore necessary to compare the velocity decay constant C_u and the jet spreading rate C_z to experimental data. Fig. 9(left) shows that over the whole Reynolds number range the agreement is very satisfactory and that both constants decrease monotonically with increasing Reynolds number. It must be mentioned that the flow has not yet reached the fully self-similar state for the lowest Reynolds number. Furthermore it is evident that, concerning these quantities, the flow is close to a converged state although it is not yet reached. Comparing our spreading rate C_z with the numerical findings of Stanley et al. (2002) (see Table 1), their value appears a little bit low (compared for example with GW), especially with respect to the fact that C_z decreases with increasing *Re* and that most of the experiments are performed at higher *Re*.

The constants $C_{u,0}$ and $C_{z,0}$ in (14) and (15) respectively are called the virtual origin of the jet. NÖ found that the dependence of $C_{u,0}$ was not systematic and varied in the range from $-4.2, \ldots, 1.3$. $C_{z,0}$ was approximately 6 for all Reynolds numbers except for $Re = 6000$ in which case the value dropped to 0.6. Our observations showed (see Fig. 9(right)) that basically the virtual origin approaches more and more the nozzle with increasing Reynolds number. Therefore it must be

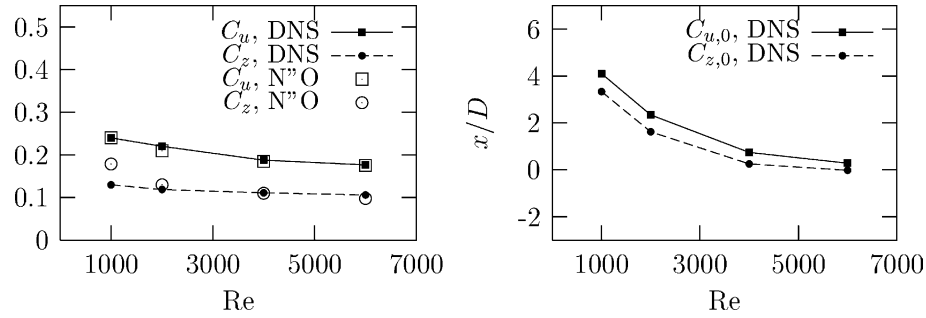

Fig. 9. Jet spreading rate and velocity decay constant for different Reynolds numbers (left). Virtual origin of the jet according to formula (14) and (15) respectively (right).

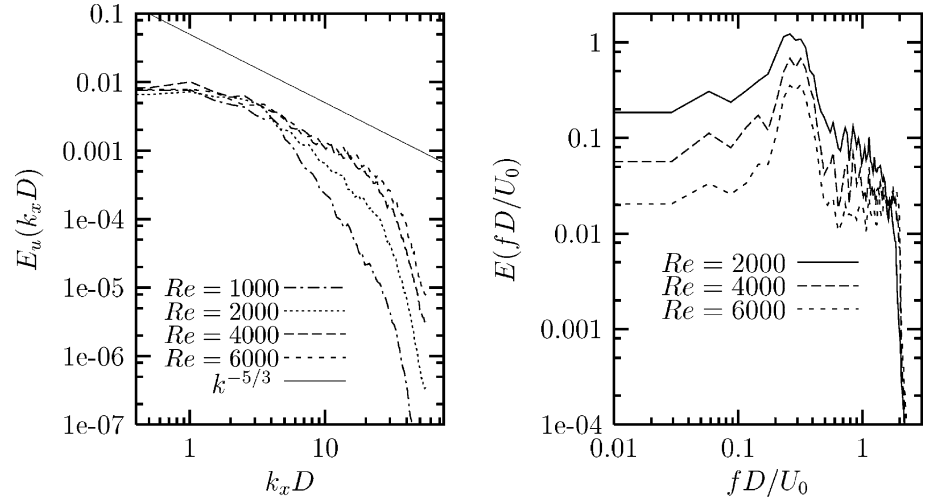

Fig. 10. Spatial power spectrum at the jet axis for different Reynolds numbers (left). Temporal energy spectrum for different Reynolds numbers, evaluated at $x/D = 2.5$ in the shear layer (right).

concluded that the scatter in the experimental data is due to a change in the inflow conditions corresponding to different Reynolds numbers, which are held constant in our simulations.

Let us now draw our attention to some spectral characteristics of the plane jet. Fig. 10(left) shows a spatial power spectrum. The velocity signal in the range $3.5 \leqslant x/D \leqslant 17.5$ is multiplied by a Hanning Window, Fourier transformed and averaged over 100 samples. The inertial subrange and the dissipation range can clearly be seen. Furthermore it is interesting to observe that the spectrum approaches, in the inertial subrange, the theoretical limit of $k^{-5/3}$ when increasing the Reynolds number.

There is strong evidence that the initial jet growth is controlled by large vortical structures which are formed near the boundaries of the jet (see for example Thomas and Goldschmidt, 1986). Therefore as in Namer and Ötügen (1988) we evaluated temporal power spectra in the shear layer at the position $x/D = 2.5$. Normalizing the most amplified frequency with the jet exit velocity and the nozzle diameter Namer and Ötügen (1988) obtained a Strouhal number $St = fD/U_0$ of 0.273 constant over the whole Reynolds number range. The meaning of this finding is that the number of vortices formed per unit length is unaffected by the Reynolds number. This is confirmed quantitatively and qualitatively by our simulations (see Fig. 10(right)).

The existence of large coherent structures becomes also obvious from the autocorrelation functions in the near field of the jet shown in Fig. 11(left). Strong undershoots can be seen until the end of the potential core at approximately $x/D = 5$. In the far field of the jet the autocorrelation functions collapse onto a single curve when normalized with the jet half-width (see Fig. 11(right)). The integration of R_{uu} yields a longitudinal length scale of approximately $L_x/z_{1/2} = 0.56$. Compared to the findings of GW $L_x/z_{1/2} = 0.47$, the agreement is satisfactory. Stanley et al. (2002) report a higher value of $L_x/z_{1/2} = 0.65$.

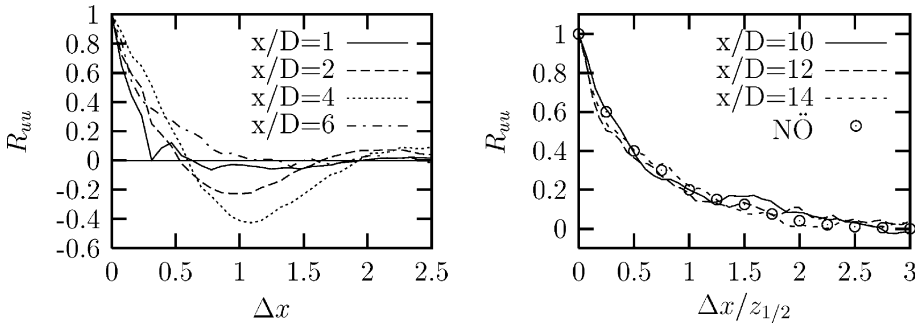

Fig. 11. Autocorrelation functions with streamwise (normalized) separation at different axial positions.

5. Conclusions

A direct numerical simulation of plane turbulent jets at moderate Reynolds numbers has been performed. Special attention has been drawn on the influence of the Reynolds number as well as the inflow conditions on the evolution of the plane jet. Concerning the first parameter it is observed that the flow is not independent of the Reynolds number but close to a converged state at $Re = 6000$, at least for the quantities under consideration in this work. The influence of the inflow conditions on the jet characteristics is so strong and long living (here observed until the end of the computational domain) that, for example, the value of the jet spreading rate can lie between 0.08 for a channel flow profile and more than 0.106 for the smoothed top-hat profile together with adequate fluctuations, generated by a newly developed method. Both facts together can explain a lot of the experimental scatter observed in the literature. A consequence is that more care must be taken in future, when comparing DNS results with LES results which were not performed with the same code and the same boundary conditions or when comparing simulation results with experimental or numerical findings at different Reynolds numbers. Furthermore there is strong need for a thorough documentation of the inflow conditions for future experimental and numerical work, which goes beyond mean quantities. Although these conclusions are drawn for the case of a plane jet, the results are probably also valid for other kind of flows.

Acknowledgements

The authors are grateful for the financial support by the DFG Schwerpunktprogramm (Fluidzerstäubung und Sprühvorgänge) and SFB 568 (Project A4).

References

Batchelor, G., 1953. The Theory of Homogeneous Turbulence. Cambridge University Press.

Bonnet, J., Moser, R., Rodi, W., 1998. AGARD advisory report 345, A Selection of Test Cases for the Validation of Large Eddy Simulations of Turbulent Flows. AGARD 1998, 7 Rue Ancelle, 99200 Neuilly-sur Seine, France, p. 35 (Chapter 6.3, Jets).

Glaze, D., Frankel, S., in press. Stochastic inlet conditions for large eddy simulation of a fully-turbulent jet. AIAA J.

Gutmark, E., Wygnanski, I., 1976. The planar turbulent jet. J. Fluid Mech. 73, 465–495.

Hinze, J., 1959. Turbulence. McGraw-Hill.

Hussain, A., Clark, R., 1977. Upstream influence on the near field of a plane trubulent jet. Phys. Fluids 20 (9), 1416–1426.

Hussein, H., Capp, S., George, W., 1994. Velocity measurements in a high-reynolds-number, momentum-conserving axisymmetric, turbulent jet. J. Fluid. Mech. 258, 31–75.

Klein, M., Sadiki, A., Janicka, J., September 2000. Direct numerical simulations of plane turbulent jets at moderate reynolds numbers. In: 20th IUTAM Congress, ICTAM 2000, Chicago.

Klein, M., Sadiki, A., Janicka, J., June 2001. Influence of the boundary conditions on the direct numerical simulation of a plane turbulent jet. In: TSFP2, 2nd International Symposium on Turbulence and Shear Flow Phenomena, vol. I. Stockholm, pp. 401–406.

Klein, M., Sadiki, A., Janicka, J., 2003. A digital filter based generation of inflow data for spatially developing direct numerical or large eddy simulations. J. Comput. Phys. 186, 652–665.

Lee, S., Lele, S., Moin, P., 1992. Simulation of spatially evolving compressible turbulence and the application of taylors hypothesis. Phys. Fluids A 4, 1521–1530.

Lund, T., Wu, X., Squires, D., 1998. Generation of turbulent inflow data for spatially-developing boundary layer simulations. J. Comput. Phys. 140, 233–258.

Mengler, C., Heinrich, C., Sadiki, A., Janicka, J., June 2001. Numerical prediction of momentum and scalar fields in a jet in cross flow: comparison of LES and second order turbulence closure calculations. In: TSFP2, vol. II. Stockholm, pp. 425–430.

Namer, I., Ötügen, M., 1988. Velocity measurements in a plane turbulent air jet at moderate Reynolds numbers. Exp. Fluids 6, 387–399.

Nobach, H., 1997. Verarbeitung stochastisch abgetasteter Signale. Ph.D. Thesis, Universität Rostock.

Panchapakesan, N., Lumley, J., 1993. Turbulence measurements in axisymmetric jets of air and helium. part 1. Air jet. J. Fluid Mech. 246, 197–223.

Ramaprian, B., Chandrasekhara, M., 1985. Lda measurements in plane turbulent jets. Trans. ASME 107, 264–271.

Ribault, C.L., Sarkar, S., Stanley, S., 1999. Large eddy simulation of a plane jet. Phys. Fluids 11, 3069–3083.

Stanley, S., Sarkar, S., 2000. Influence of nozzle conditions and discrete forcing on turbulent planar jets. AIAA J. 38, 1615–1623.

Stanley, S., Sarkar, S., Mellado, J., 2002. A study of the flow field evolution and mixing in a planar turbulent jet using direct numerical simulation. J. Fluid Mech. 450, 377–407.

Thomas, F., Goldschmidt, V., 1986. Structural characteristics of a developing turbulent planar jet. J. Fluid Mech. 163, 227–256.

Thomas, F., Prakash, K., 1991. An experimental investigation on the natural transition of an untuned planar jet. Phys. Fluids 3, 90–105.

Wygnanski, I., Fiedler, H., 1975. Some measurements in the self-preserving jet. J. Fluid Mech. 38, 577–612.